

SoloPose: One-Shot Kinematic 3D Human Pose Estimation with Video Data Augmentation

David C. Jeong, Hongji Liu, Saunder Salazar, Jessie Jiang, Christopher A. Kitts
Santa Clara University

dcjeong@scu.edu, hliu4@scu.edu, ssalazar@scu.edu jjiang3@scu.edu, ckitts@scu.edu

Abstract

While recent two-stage many-to-one deep learning models have demonstrated great success in 3D human pose estimation, such models are inefficient ways to detect 3D key points in a sequential video relative to one-shot and many-to-many models. Another key drawback of two-stage and many-to-one models is that errors in the first stage will be passed onto the second stage. In this paper, we introduce *SoloPose*, a novel one-shot, many-to-many spatio-temporal transformer model for kinematic 3D human pose estimation of video. *SoloPose* is further fortified by *HeatPose*, a 3D heatmap based on Gaussian Mixture Model distributions that factors target key points as well as kinematically adjacent key points. Finally, we address data diversity constraints with the 3D *AugMotion Toolkit*, a methodology to augment existing 3D human pose datasets, specifically by projecting four top public 3D human pose datasets (*Humans3.6M*, *MADS*, *AIST Dance++*, *MPI INF 3DHP*) into a novel dataset (*Humans7.1M*) with a universal coordinate system. Extensive experiments are conducted on *Human3.6M* as well as the augmented *Humans7.1M* dataset, and *SoloPose* demonstrates superior results relative to the state-of-the-art approaches.

1. Introduction

Monocular pose estimation takes 2D images or videos as input, and generates 2D or 3D coordinates of skeletal key points. This task has a variety of applications such as action recognition, sports analysis, medical rehabilitation, and collaborative robotics [16, 17]. Models to generate 2D skeleton key points have been greatly improved in recent years [2, 8, 12, 20, 25, 27], but there is still room for improvement for 3D human pose estimators due to the following.

First, there is a lack of high-quality 3D datasets for pose estimation. Many pose estimation models [2, 8, 12, 20, 25, 27] are trained on *Human3.6M* [5], which is limited in image resolution and data diversity (e.g., limited actors, ac-

tions) [3]. The disproportionate use of the *Human3.6M* dataset constrains the accuracy and efficiency of existing 3D human pose estimation models. The natural solution to such data diversity issues is to train on alternative datasets, such as *MADS* [26], *AIST Dance++* [23] and *MPI INF 3DHP* [11]. Of course, each additional dataset requires respective training due their unique marker format, data distribution, and ground truth. Ultimately, addressing data diversity issues with alternative datasets presents added costs in training time and performance accuracy on data in-the-wild, thus severely constraining downstream applications.

Second, most 3D human pose estimators are two-stage models [2, 8, 12, 20, 25, 27] that are a) highly dependent on the accuracy of 2D estimators, and b) solely take 2D skeletal keypoints as input, thus omitting valuable contextual information needed for computational efficiency during 3D human pose estimation.

Finally, recent pose estimators utilize transformers as the deep learning network [2, 8, 12, 20, 27]. Most video-based models process frames in a time-consuming many-to-one approach [8, 20, 27], which take multiple frames as input but select solely the middle frame to estimate coordinates, neglecting frames at the beginning and end of videos.

In sum, 3D human pose estimators are constrained by limitations in 1) 3D human pose datasets, 2) two-stage models, and 3) many-to-one approaches. To address these challenges, we propose the following contributions:

1. We introduce *SoloPose*¹, a cost-efficient one-shot, many-to-many spatio-temporal transformer model of 3D human pose estimation that takes frame sequences of monocular 2D video as input to directly estimate 3D key point coordinates.
2. We propose the *3D AugMotion Toolkit* to augment existing datasets (e.g., *Humans3.6M*, *MADS*, *AIST Dance++*, *MPI INF 3DHP*) by increasing diversity and reducing noise, yielding an augmented dataset that we refer to as *Humans7.1M*.

¹All relevant code and documentation may be found on GitHub: <http://tinyurl.com/3m488z83>

Table 1. Complexity Hierarchy in 3D Human Pose Estimation

	single person	3D human pose	video input	single stage	many-to-many	data augmentation	heatmap
STCFormer [22]	✓	✓	✓	✗	✗	✗	✗
P-STMO [20]	✓	✓	✓	✗	✗	✗	✗
MHFormer [8]	✓	✓	✓	✗	✗	✗	✗
PoseFormer [27]	✓	✓	✓	✗	✗	✗	✗
Coarse-to-fine [13]	✓	✓	✗	✓	✗	✗	✓
Geometry-Aware [18]	✓	✓	✗	✓	✗	✓	✗
MeTRAbs [19]	✓	✓	✗	✓	✗	✗	✗
HEMIlets [28]	✓	✓	✗	✓	✗	✗	✓
Our SoloPose	✓	✓	✓	✓	✓	✓	✓

3. Finally, we introduce *HeatPose*, a 3D heatmap based on GMM, which represents kinematically adjacent information of each given target key point, including key point labels, distance, and direction. We utilize cross entropy as a loss function in SoloPose instead of MSE loss to improve the accuracy of 3D coordinates.

We structure the current work as follows. First, we discuss related work of the current state-of-the-art in monocular 3D human pose estimation as well as prevailing 3D human pose video datasets. Second, we introduce the 3D Augmotion Toolkit, a methodology to augment 3D human pose datasets using universal coordinate systems, which we leverage to generate our Humans7.1M dataset. Third, we introduce SoloPose, a one-shot, many-to-many spatio-temporal transformer for 3D human pose estimation, which is fortified by our 3D GMM-based heatmap (*HeatPose*). Next, we demonstrate SoloPose’s performance by comparing SOTA methods, as well as comparing existing Humans3.6M and our Humans7.1M datasets. Finally, we conduct ablation studies to test our contributions, namely *HeatPose* (i.e., 3D Gaussian heatmap) and AugMotion (i.e., 3D human pose data augmentation).

2. RELATED WORK

In the following, we present the constraints and limitations in existing a) 3D human pose estimation model methodologies, namely an observed prevalence of many-to-one video frame approaches, two-stage, and key point regression methodologies, and b) 3D human pose datasets.

2.1. 3D human pose Estimation of Videos

2.1.1 Many-to-One Models

While single-image pose estimation performance is well-established [6, 13, 21], pose estimation of sequences of multiple frames (i.e., videos) is the focus of recent research [2, 8, 12, 20, 25, 27]. Pose estimation of sequential frames leverages temporal information to address occlusion issues. That being said, most video-based pose estimation

models take a many-to-one approach [2, 8, 12, 20, 25, 27], which estimates key points for a solitary middle frame among the input frames within a fixed sequence of frames, thus impacting model complexity and learning efficiency.

2.1.2 Two-stage 3D Human Pose Estimation Methods

While previous work [6, 13, 21] propose one-shot methodologies to boost efficiency and accuracy, these models have thus far solely utilized a single image inputs, preventing effective detection of temporal information.

Alternatively, video-based 3D human pose estimation largely utilize two-stage methods of lifting 3D coordinates after generating 2D coordinates with off-the-shelf 2D pose estimators, offering compatibility with any 2D pose estimation method. For instance, Skeletal graph neural networks (SGNN) [25] use off-the-shelf 2D key point detectors [2, 12] to obtain the 2D poses needed to derive 3D human poses. Despite improved performance over previous models, SGNN yet lacks spatial depth perception of objects in a scene, which is addressed by PoseFormer [27] using a spatial-temporal transformer structure. That said, PoseFormer is constrained in learning 2D-to-3D spatial and temporal correlations, and requires more training data than CNNs.

MHFormer [8] addresses the optimization constraints of PoseFormer by synthesizing an ultimate pose from learning spatio-temporal representations multiple plausible pose hypotheses. However, MHFormer requires a large high-quality data to maintain high performance, which P-STMO [20] addresses with a self-supervised pre-training method, but is ultimately constrained by the quadratic growth of its computational cost as the number of video sequences increases, given its many-to-one methodology. Most recently, STCFormer [22] presents a state-of-the-art spatio-temporal criss-cross attention (STC) block by decomposing correlation learning across space and time to increase processing speed. Nonetheless, STCFormer [22] is limited by the quality of 2D pose estimators, as it is a two-stage method.

2.1.3 Heatmap Representations of Pose Estimation

A recent development in pose estimation has been to configure models to learn heatmap estimation as an alternative to key point regression [13, 19, 28]. Coarse-to-fine [13] builds 3D Gaussian distributions centered around the ground truth position to solve non-linear problem of direct 3D coordinate regression. Based on coarse-to-fine [13], HEMlets [28] incorporate the kinematic information of a parent joint and a child joint (Part-Centric Heatmap Triplets) to improve accuracy of 3D key points estimation. However, both Coarse-to-fine and HEMlets use MSE as loss functions, leading to non-convex problems.

RLE [7] replaces the MSE loss function with likelihood loss function, resulting in an elevated time complexity. Thus, keypoint transformer [4] utilizes the cross-entropy loss of 3D heatmap instead of likelihood loss. However, this 3D heatmap did not consider adjacent joints' kinematic connections, which prevents the model from distinguishing between different key points. Though HEMlets [28] considers adjacent key points, its triplet structure at most include three key points, missing connections where more than three key points are kinematically connected.

2.2. Dataset Constraints

2.2.1 3D Human Pose Estimation Datasets

3D datasets for pose estimation are difficult to generate, as motion capture systems must be used to generate accurate 3D coordinates as ground truth. However, mocap-generated datasets ultimately cannot contain data in the wild. Recent developments have seen novel approaches to estimate ground truth data using algorithms, which made 3D human pose datasets easier to make, but ground truth of such datasets tend to be less accurate, posing new problems for training.

Human3.6M [5] is the first ever large-scale dataset that uses motion capture equipment to track accurate 3D coordinates while a number of actors performing different daily life movements. MADS [26], developed by City University of Hong Kong, uses the same approach as Human3.6M in a smaller scale and includes movements in martial arts, dancing and sports. AIST Dance++ [23] is a recent dataset with high-definition recording of dancing of multiple genres. Its difference from the first two datasets is that it is marker-free, meaning algorithms are used for ground truth. MPI INF 3DHP [11] is a 3D marker-based dataset as an extension of the classic 2D dataset MPII.

2.2.2 Existing Dataset Limitations

Existing 3D human pose datasets are lacking in scale and diversity. First, the performance of the vision transformers may be constrained by the limited number of frames in the

datasets. For instance, AIST Dance ++ [23] is 2.4 times larger than Human3.6M [5], but it only has 12760 videos.

Apart from a data size limitations, existing 3D human pose datasets are in lacking in diversity, negatively impacting in-the-wild applications. Most existing 3D human pose datasets are shot in a studio with fixed lighting, background, and the same set of actors. For instance, AIST Dance++ [23] has 10 dance genres and 30 dancers.

2.2.3 Data Augmentation Methodologies

Recent work [18, 23] has developed novel data augmentation methodologies to address data diversity limitations of existing 3D human pose estimation datasets, namely by scaling dataset size by standardizing different datasets to feed into one training process. [15, 18].

Three such data augmentation precedents are observed. The first involves using handcrafted rules in skeletal joints to manually harmonize differences between datasets (HumanEva-I, Human3.6M, and Panoptic Studio) into one combined dataset [15]. However, handcrafted rules are susceptible to errors and similar manual configurations are required to apply such a methodology onto other datasets. A second approach [24] is to standardize reference systems based on the relative rotation between camera viewing direction and the orientation of the torso. However, this approach is vulnerable to errors during conversion from camera to global coordinate systems. A third method of dataset augmentation merges dozens of datasets into one training process with a latent key point set serving as ground truth [18]. Such a learned latent key point set, however, leads to data imbalance and is further constrained in performance by the complexity of a given task.

3. 3D AugMotion Toolkit: Dataset Augmentation Methodology

Acknowledging the lack of diversity and in-the-wild data in existing 3D human pose datasets, we introduce the 3D AugMotion Toolkit, a data augmentation methodology to merge existing 3D human pose datasets into a single dataset with the highest number of frames and diversity to date. The current work applies the augmentation methodology on four frequently utilized datasets, namely Human3.6M [5], MADS [26], AIST Dance++ [23] and MPI INF 3DHP [11]. That said, the 3D AugMotion Toolkit is applicable to any 3D human pose estimation dataset.

It is essential for all datasets to be projected onto a universal coordinate system to be properly used by models as ground truth data. Naturally, the model would be unable to minimize loss if a single key point could have multiple coordinates. Therefore, the first challenge is to address discrepancies between datasets' reference systems as each dataset maintains its own coordinate system. That is, ground truth

data of each dataset comes with unique camera-configured coordinates and global coordinates, respectively.

As 3D human pose datasets are typically captured with multi-camera studio set-ups, the perspective and configurations of each camera dictate its coordinate system. Naturally, each camera maintains its own unique camera-specific coordinate system. Most datasets [5, 11, 23, 26] compute translation and rotation matrix to standardize the coordinates of each camera within the multi-camera setup onto a global coordinate system. However, global coordinate systems of 3D human pose datasets are not consistent with each other, meaning they require standardization to locate the same key point with the same coordinates.

Global reference systems within the same dataset, however, are also susceptible to errors. For instance, coordinates for the same frame of movement within the Humans3.6M dataset are taken from different camera perspectives that yield misaligned and non-overlapping key point representations of a subject when converted to global coordinates. The four key point skeletons in Fig. 1 represent the same pose from the same subject taken from multiple perspectives, but each are clearly misaligned when converted to global 3D coordinate systems. The lack of overlapping alignment suggests a need for a standard to universalize all camera reference systems with key frames.

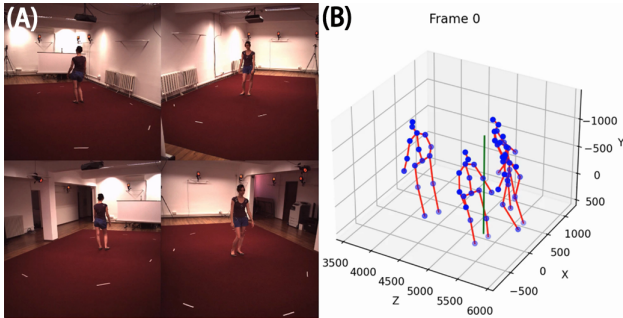


Figure 1. This example from the Human3.6M dataset (A) shows how the conversions to global coordinate systems from unique camera parameters are susceptible to errors. The four key point skeletons (B) represent the same pose from the same subject taken from multiple perspectives, but each are misaligned when converted to global 3D coordinate systems.

To address the coordinate system problems above, the proposed methodology is to 1) select key frames serving as benchmark, 2) use key frames and the proposed approach to establish a universal coordinate system, and 3) utilize the Kabsch Algorithm to project all other frames onto the established universal coordinate system.

3.1. Key Frames

The proposed universal coordinate system defines the upward direction as perpendicular to the ground as the pos-

itive direction of the z-axis. We select as key frames where the upper body of the pose is perpendicular to the ground. We utilize k -means clustering to find qualified key frames with 3 clusters and select the cluster center frame of the largest cluster as the key frame for each video.

3.2. Methodology for Defining a Universal Coordinate System

Unique coordinate systems are defined by origin, as well as positive orientation of the x , y , and z axis. In the proposed methodology, we further define the *origin* as the midpoint between left shoulders and right shoulders, the *y-axis positive orientation* as left-shoulder-to-right-shoulder vectors, the *z-axis positive orientation* as origin-to-pubis vectors, and the *x-axis positive orientation* as face directions.

We further select left shoulders, right shoulders, and pubises as *reference key points* as shown in red in Fig. 3. Based on the definitions above, the left shoulder key point and the right shoulder key point would be on the y - z plane symmetric to each other while the pubis key point is on the z axis. Before determining coordinates of the reference key points to define unit length and used for the Kabsch algorithm, we compute the ratio of the shoulder to shoulder distance (i.e., width) to the distance from the shoulder to shoulder midpoint to the pubis to properly represent poses in the coordinate system. Refer to Equation (1) for further detail.

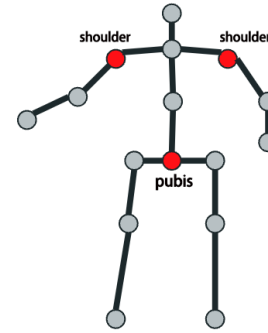


Figure 2. Red points represent 3D reference key points, namely left shoulder, right shoulder, and pubis.

After taking the average of all datasets to compute the ratio of the distance $d(p_{sl}^i, p_{sr}^i)$ to the distance $d(p_{ms}^i, p_p^i)$, we then define the left shoulder at $(-1,0,3)$, the right shoulder at $(1,0,3)$, and the pubis at $(0,0,0.5)$ to establish the universal coordinate system.

$$M_s = \frac{1}{N} \sum_{i=1}^N d(p_{sl}^i, p_{sr}^i) \tag{1}$$

$$M_{sp} = \frac{1}{N} \sum_{i=1}^N d(p_{ms}^i, p_p^i)$$

Where M_s is the average distance from left shoulder to right shoulder; M_{sp} is the average distance from the middle of two shoulders to pubis; $d()$ is the distance function; N is the number of frames in all datasets; p_{sl} is the left shoulder key point; p_{sr} is the right shoulder key point; p_{ms} is the midpoint between two shoulders; p_p is the pubis key point.

3.3. Kabsch Algorithm

The last step of our dataset augmentation methodology is to use the Kabsch Algorithm (KA) [1] to compute the rotation matrix and translation matrix for projection. KA finds the optimal rotation and translation of two sets of points in N-dimensional space with linear and vector algebra to minimize root-mean-square deviation (RMSD) between them. KA does translation, computation of a covariance matrix, and computation of the optimal rotation matrix sequentially. The translation matrix T is computed by subtracting point coordinates from the point coordinates of the respective centroid. The second step consists of calculating a cross-covariance matrix H when P and Q are seen as data matrices using the following summation notation:

$$H_{ij} = \sum_{k=1}^N P_{ki} Q_{kj}, \quad (2)$$

The last step is to calculate the optimal rotation R by using singular value decomposition (SVD):

$$\begin{aligned} H &= U \Sigma V^T \\ d &= \text{sign}(\det(VU^T)) \\ R &= V \begin{pmatrix} 1 & 0 & 0 \\ 0 & 1 & 0 \\ 0 & 0 & d \end{pmatrix} U^T \end{aligned} \quad (3)$$

Now that we have the translation matrix T and the optimal rotation R to project the key frame into the global standard:

$$R \times A + t = B \quad (4)$$

Where A represents the original coordinates of the key frame's key points; B represents the projected coordinates of the key frame's key points.

4. SoloPose: One-shot 3D human pose estimation network

4.1. Spatio-temporal transformer

We propose a one-shot many-to-many transformer-based method to extract feature maps from spatial and temporal data, as shown in Fig. 3. Spatial information is represented by intra-frame content within respective frames, whereas temporal information is represented by inter-frame content between multiple frames along a time-series.

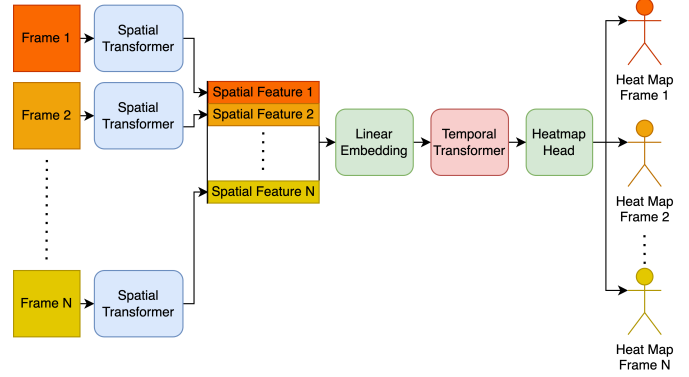


Figure 3. The framework of our proposed network, *SoloPose* spatio-temporal transformer.

We first utilize the spatial transformer for each input frame to extract the spatial feature maps of each input frame. Then we utilize the temporal transformer with the spatial feature maps as the input to extract the temporal feature maps. Finally, we propose a heatmap task head (i.e., layer extraction) to convert temporal feature maps into our proposed 3D heatmap, which we discuss later.

For the spatial transformer, we apply the pre-trained model, CLIP [14], which has been pre-trained on an extensive dataset containing images and their corresponding text descriptions. Each frame goes through the spatial transformer to obtain spatial feature maps, whose size is $1 \times 200 \times 192$. Then, we concatenate all the spatial feature maps along the channel dimension resulting in an output size that is $n \times 200 \times 192$, where n is the number of frames in one clip.

For the temporal transformer, we apply a linear embedding layer to flatten the spatial feature maps into 2D tokens. Our temporal transformer is mostly based on Swin transformer blocks [9] with an update to 3D relative position embedding. We calculate 3D relative distances between any two input tokens, as the position index to obtain the value of \mathbf{B} from the 3D bias matrix $\hat{\mathbf{B}}$, which contains relative weights that will be updated during the training process:

$$A(\mathbf{Q}, \mathbf{K}, \mathbf{V}) = \text{Softmax} \left(\mathbf{QK}^T / \sqrt{d} + \mathbf{B} \right) \times \mathbf{V}, \quad (5)$$

where $\mathbf{Q}, \mathbf{K}, \mathbf{V}$ are the query, key and value matrices.

In the last layer, we apply a heatmap task head by 3 convolutional neural networks to reshape the temporal feature maps into our proposed 3D heatmap, which is a probability result introduced in the next section.

4.2. HeatPose: 3D Gaussian heatmap

We propose a *HeatPose*, a 3D heatmap based on Gaussian mixture model (GMM) [10]. Although conventional GMMs do not factor weights into its various Gaussian dis-

tributions, we adapted GMM in HeatPose to represent varying degrees of probabilistic proximity to the ground truth of a given target key point across different weights of Gaussian distributions. In other words, we generated Gaussian distributions for each key point, each of which are evaluated for closeness to the ground truth. The maximum value of a given Gaussian distribution would be the actual ground truth positioning of its corresponding target key point. We refer to this target-based distribution as the main 3D Gaussian Distribution, and it is the primary mechanism of HeatPose.

However, HeatPose is also supplemented by factoring information regarding key points that are kinematically adjacent from a given target key point (e.g., direction, distance), which we represent with a finite number of target-adjacent distributions that we refer to as the side 3D Gaussian Distributions.

Side 3D Gaussian distribution may be understood by hypothetically considering the neck key point as a given target key point, as seen in 5 (A). In this example, the neck key point is kinematically adjacent to the key points of the shoulder, head, and pubis Fig. 5 (A). The application of kinematically adjacent key points in HeatPose serves to reflect closer-to-reality distributions as the probability of a key point is affected by key points nearby. As seen in Fig. 4, we present a comparison of conventional 3D heatmaps without kinematic information (left) and HeatPose with application of kinematically adjacent keypoints (right). The distinction between the application of kinematically adjacent key points and conventional 3D heatmaps without such kinematic information is illustrated in Fig. 4

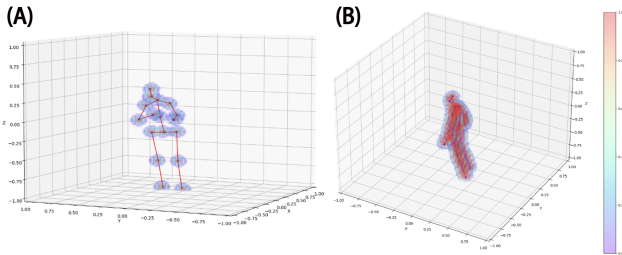


Figure 4. The left figure (A) is the 3D heatmap of human key points [13]. The right figure (B) is our proposed heatmap, HeatPose. Each sphere in the right figure represents a key point with discrete points with unique probability distributions represented with different colors, with red signifying close to 1 probability as a key point, and purple signifying close to 0 probability.

For each target key point’s main 3D Gaussian distribution, we set coordinates of the target key point as μ_{main} , and a specified covariance matrix as σ_{main} to represent the ground truth of a given target key point. To decide each target key point’s side 3D Gaussian distribution, we compute the number N_{side} of side Gaussian distributions in advance

to represent the distance $D(P_t, P_a)$ between a given target key point and a kinematically adjacent key point following the Equation 6, where c is a constant. Thus, the longer the distance between two adjacent key points, the more side Gaussian distributions there will be to represent kinematic information, so that each key point is unique represented by a different distribution:

$$N_s = \frac{D(P_t, P_a)}{c} \tag{6}$$

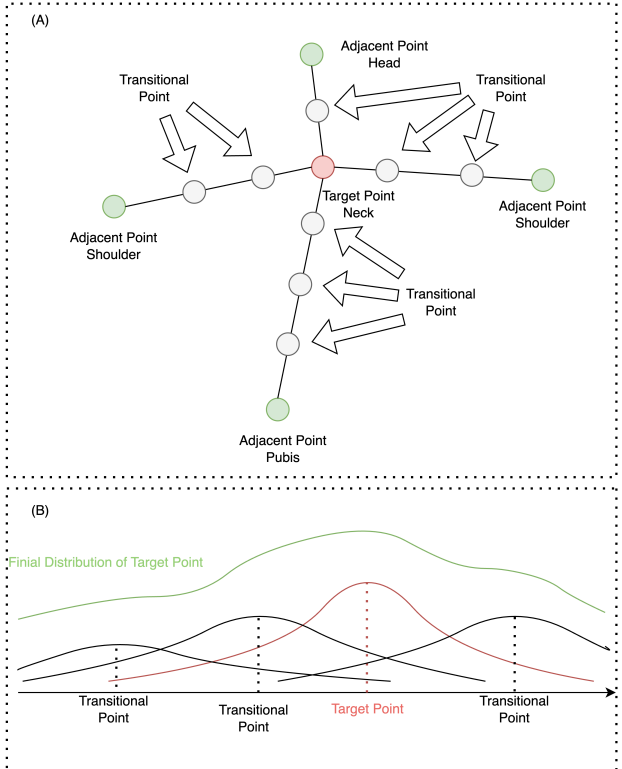


Figure 5. HeatPose visual summary. The upper figure (A) demonstrates the kinematically adjacent key points if we hypothetically considered the neck key point as the target key point. Adjacent key points are green and transitional points are gray. The lower figure (B) is an example of key points with two adjacent points, with the final results of the Gaussian Mixture Model distribution (GMM) of target points represented by the green line. The red line is the main 3D Gaussian distribution in GMM. And the 3 black lines are the side 3D Gaussian distributions in GMM.

Once we determine a finite number N_{side} of side 3D Gaussian distributions for each adjacent key point, we compute coordinates of N_p transitional points located between the target key point and an adjacent key point. As shown in Fig. 5, the first transitional point in N_s number of transitional points is c euclidean distance away from a given target key point. Each subsequent transitional point is c distance away from the previous transitional point. For the i th

side 3D Gaussian distributions, we set the coordinates of i th middle points as μ_{side}^i and set σ_{side}^i by Equation 7, where $i = 1, 2, \dots, N_s$.

$$\delta_{side}^i = i^2 \cdot \delta_{main} \quad (7)$$

A larger i value represents greater distance from the target key point, thus representing a less influence of the side Gaussian distribution on the target key point.

Once we build a Gaussian mixture model (GMM), we generate volumetric size $w \times h \times d$, which is discretized uniformly across each dimension. While conventional 3D heatmaps build a volume for each key point, HeatPose computes the probability of voxels of all key points into one volumetric representation, as seen in Equation 8:

$$P(x) = \frac{\mathcal{N}(x | \mu_{main}, \delta_{main}^2) + \sum_{i=1}^{N_s} \mathcal{N}(x | \mu_{side}^i, \delta_{side}^i{}^2)}{MAX} \quad (8)$$

where \mathcal{N} is Gaussian distribution, MAX stands for the maximum probability of voxels in the volume.

Based on Equation 8, we compute the cross-entropy between the output of our SoloPose and HeatPose, converted from the ground truth as our model’s loss function. Departing from existing 3D heatmaps that use MSE loss functions, using a cross-entropy loss function methodology avoids non-convex problems. That is, such cross-entropy models can easily converge because targeting the distribution of each key point affords the handling of noise in ground truth. HeatPose’s application of GMM as opposed to the single Gaussian distribution used conventional 3D heatmaps leads to more accurate representations and coordinate estimates.

As we set up increasingly larger σ for the side Gaussian distributions with regard to the corresponding main Gaussian distribution, we can easily find the maximum of voxels’ probability shown in Fig. 5 (B) to convert our HeatPose back to the 3D keypoints’ original coordinates.

5. Experiments and results

5.1. Datasets

With the AugMotion dataset augmentation method, we merge four datasets: Human3.6M [5], MADS [26], AIST Dance++ [23] and MPI INF 3DHP [11] as shown in Fig 6. Notably, we set the Human3.6M Testing Dataset as one of the independent testing datasets for a fair evaluation with SOTA models, which is not merged into our Humans7.1M dataset. The number of Human3.6M, MADS, AIST Dance++ and MPI INF 3DHP shown in Fig 6, is the number of final clips as input data of our SoloPose for training in each dataset, which is pre-processed by a sliding window with a step size of 16. From the rest of the four datasets collectively, we randomly choose 331,875 clips as

the training dataset, 94,821 clips as the validation dataset, and 47,412 clips as our Humans7.1M testing dataset.

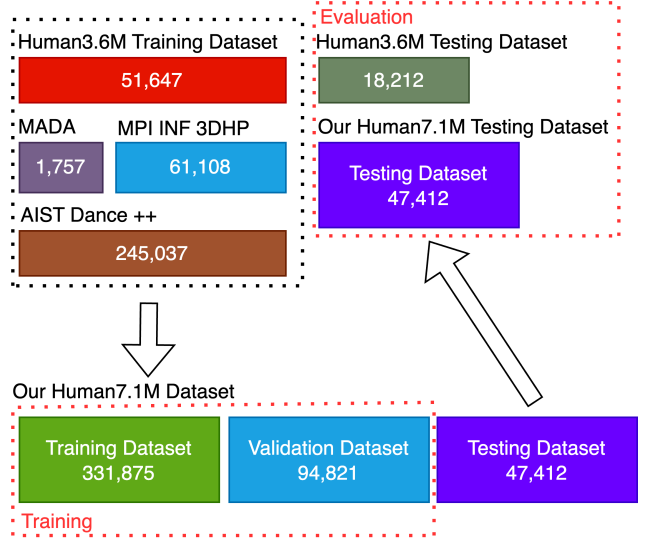


Figure 6. 3D human pose Dataset and our training, validation, and testing dataset with number of unique video clips. 7.1M is the number of frames in our augmented dataset.

5.2. Evaluation Metrics

We use the mean per joint position error (MPJPE) and Procrustes MPJPE (P-MPJPE) to evaluate two SOTA models and our SoloPose.

5.3. Comparison with the State-of-the-art

We compare the proposed model with the best-performing SOTA methods, P-STMO [20] and STCFormer [22], which are pre-trained on the Human3.6M training dataset. We test all methods on our Humans7.1M testing dataset as well as on the Human3.6M Testing dataset, which do not overlap. Both P-STMO and STCFormer are two-stage methods that choose CPN (Cascaded Pyramid Network) [2] to generate 2D coordinates as second-stage input, and 2D ground truth as input to test model’s performance. We evaluate these two models with CPN-generated 2D estimates or 2D ground truth as input, respectively. Notably, 2D ground truth as input gives the comparative models an unfair advantage because it provides additional information unavailable to the proposed one-shot method. Besides, it is impossible for any pose estimation model to obtain 2D ground truth when applied on real-world in-the-wild data. As such, we mainly compare our model against performance with CPN estimates as input but we still include GT performance for reference.

As shown in Table 2, our SoloPose achieves the highest performance of MPJPE and P-MPJPE on the Humans7.1M

Table 2. Results on different testing datasets

Method	Our Humans7.1M testing dataset		Human3.6M testing dataset	
	MPJPE	P-MPJPE	MPJPE	P-MPJPE
P-STMO w/ CPN [20]	53.1	46.9	42.1	34.4
STCFormer w/ CPN [22]	48.3	40.3	40.5	31.8
P-STMO w/ GT [20]	36.1	18.1	29.3	12.9
STCFormer w/ GT [22]	30.5	13.1	21.3	5.8
Our SoloPose	22.7	6.9	26.0	11.5
Our SoloPose w/o HeatPose	25.1	11.0	30.7	15.8
Our SoloPose only trained on Human3.6M	47.9	38.6	38.9	29.9

testing dataset. Even when compared to SOTA methods with ground truth, our results of MPJPE and P-MPJPE are still 25.5% and 47.3% lower than the best-performing STCFormer. When evaluated on the Human3.6M testing dataset, our results of MPJPE and P-MPJPE are 35.8% and 63.8% lower than STCFormer with CPN as input, and only lower than STCFormer with ground truth as input.

5.4. Ablation Study

We designed two ablation studies to test the contributions of the proposed 3D kinematically adjacent heatmap (HeatPose) and data augmentation methodology (AugMotion) to our SoloPose performance.

5.4.1 Analysis without 3D Gaussian Heatmap

The first ablation study removes HeatPose and utilizes the traditional MSE loss function to train our proposed model. As shown in the second section of Table 2, the results of MPJPE and P-MPJPE on Human3.6M testing dataset are 15.3% and 27.2% higher than that of our SoloPose with HeatPose respectively, but it is 24.2% and 50.3% lower than STCformer with CPN.

5.4.2 Analysis without Data Augmentation

The second ablation study trains the model only on Human3.6M, in the mold of P-STMO [20] and STCFormer [22]. Our results of MPJPE and P-MPJPE are still 3.9% and 5.9% lower than the two SOTA methods on the Human3.6M testing dataset, which demonstrates that our SoloPose model is more effective than current SOTA methods. When tested on the Human3.6M testing dataset, the second ablation study’s MPJPE result increases by 12.9 as opposed to the increase of 4.7 observed with the first ablation study, thus demonstrating that our proposed data augmentation methodology (AugMotion) improves 3D human pose

estimation performance by efficiently enhancing data quality and diversity.

6. CONCLUSION

In this paper, we introduced SoloPose, a one-shot, many-to-many spatio-temporal transformer network for video-based 3D human pose estimation. To address limitations of high-quality 3D human pose estimation datasets, we proposed the 3D AugMotion ToolKit, a novel dataset augmentation methodology by projecting existing datasets onto a universal coordinate system. Further, we proposed HeatPose, a 3D kinematically adjacent heatmap that provide greater probabilistic key point information compared with conventional 3D heatmaps. As a result, we demonstrate our SoloPose model’s improved performance over existing SOTA models for 3D human pose estimation in both experimental evaluation and ablation. In future work, we intend to extend the model onto 3D multi-person pose estimation.

References

- [1] Sérgio Agostinho, Aljoša Ošep, Alessio Del Bue, and Laura Leal-Taixé. (just) a spoonful of refinements helps the registration error go down. In *Proceedings of the IEEE/CVF International Conference on Computer Vision*, pages 6108–6117, 2021. 5
- [2] Yilun Chen, Zhicheng Wang, Yuxiang Peng, Zhiqiang Zhang, Gang Yu, and Jian Sun. Cascaded pyramid network for multi-person pose estimation. In *Proceedings of the IEEE conference on computer vision and pattern recognition*, pages 7103–7112, 2018. 1, 2, 7
- [3] Zhiqiang Gong, Ping Zhong, and Weidong Hu. Diversity in machine learning. *Ieee Access*, 7:64323–64350, 2019. 1
- [4] Shreyas Hampali, Sayan Deb Sarkar, Mahdi Rad, and Vincent Lepetit. Keypoint transformer: Solving joint identification in challenging hands and object interactions for accurate 3d pose estimation. In *Proceedings of the IEEE/CVF Conference on Computer Vision and Pattern Recognition*, pages 11090–11100, 2022. 3

- [5] Catalin Ionescu, Dragos Papava, Vlad Olaru, and Cristian Sminchisescu. Human3.6m: Large scale datasets and predictive methods for 3d human sensing in natural environments. *IEEE Transactions on Pattern Analysis and Machine Intelligence*, 36(7):1325–1339, jul 2014. [1](#), [3](#), [4](#), [7](#)
- [6] Lei Jin, Chenyang Xu, Xiaojuan Wang, Yabo Xiao, Yandong Guo, Xuecheng Nie, and Jian Zhao. Single-stage is enough: Multi-person absolute 3d pose estimation. In *Proceedings of the IEEE/CVF Conference on Computer Vision and Pattern Recognition*, pages 13086–13095, 2022. [2](#)
- [7] Jiefeng Li, Siyuan Bian, Ailing Zeng, Can Wang, Bo Pang, Wentao Liu, and Cewu Lu. Human pose regression with residual log-likelihood estimation. In *Proceedings of the IEEE/CVF international conference on computer vision*, pages 11025–11034, 2021. [3](#)
- [8] Wenhao Li, Hong Liu, Hao Tang, Pichao Wang, and Luc Van Gool. Mhformer: Multi-hypothesis transformer for 3d human pose estimation. In *Proceedings of the IEEE/CVF Conference on Computer Vision and Pattern Recognition*, pages 13147–13156, 2022. [1](#), [2](#)
- [9] Ze Liu, Yutong Lin, Yue Cao, Han Hu, Yixuan Wei, Zheng Zhang, Stephen Lin, and Baining Guo. Swin transformer: Hierarchical vision transformer using shifted windows. In *Proceedings of the IEEE/CVF international conference on computer vision*, pages 10012–10022, 2021. [5](#)
- [10] Geoffrey J McLachlan and Suren Rathnayake. On the number of components in a gaussian mixture model. *Wiley Interdisciplinary Reviews: Data Mining and Knowledge Discovery*, 4(5):341–355, 2014. [5](#)
- [11] Dushyant Mehta, Helge Rhodin, Dan Casas, Pascal Fua, Oleksandr Sotnychenko, Weipeng Xu, and Christian Theobalt. Monocular 3d human pose estimation in the wild using improved cnn supervision. In *3D Vision (3DV), 2017 Fifth International Conference on*. IEEE, 2017. [1](#), [3](#), [4](#), [7](#)
- [12] Alejandro Newell, Kaiyu Yang, and Jia Deng. Stacked hourglass networks for human pose estimation. In *Computer Vision—ECCV 2016: 14th European Conference, Amsterdam, The Netherlands, October 11–14, 2016, Proceedings, Part VIII 14*, pages 483–499. Springer, 2016. [1](#), [2](#)
- [13] Georgios Pavlakos, Xiaowei Zhou, Konstantinos G Derpanis, and Kostas Daniilidis. Coarse-to-fine volumetric prediction for single-image 3d human pose. In *Proceedings of the IEEE conference on computer vision and pattern recognition*, pages 7025–7034, 2017. [2](#), [3](#), [6](#)
- [14] Alec Radford, Jong Wook Kim, Chris Hallacy, Aditya Ramesh, Gabriel Goh, Sandhini Agarwal, Girish Sastry, Amanda Askell, Pamela Mishkin, Jack Clark, et al. Learning transferable visual models from natural language supervision. In *International conference on machine learning*, pages 8748–8763. PMLR, 2021. [5](#)
- [15] Michał Rapedzyński, Philipp Werner, Sebastian Handrich, and Ayoub Al-Hamadi. A baseline for cross-database 3d human pose estimation. *Sensors*, 21(11), 2021. [3](#)
- [16] Edoardo Remelli, Shangchen Han, Sina Honari, Pascal Fua, and Robert Wang. Lightweight multi-view 3d pose estimation through camera-disentangled representation. In *Proceedings of the IEEE/CVF conference on computer vision and pattern recognition*, pages 6040–6049, 2020. [1](#)
- [17] Yu Rong, Takaaki Shiratori, and Hanbyul Joo. Frankmocap: A monocular 3d whole-body pose estimation system via regression and integration. In *Proceedings of the IEEE/CVF International Conference on Computer Vision*, pages 1749–1759, 2021. [1](#)
- [18] István Sárádi, Alexander Hermans, and Bastian Leibe. Learning 3d human pose estimation from dozens of datasets using a geometry-aware autoencoder to bridge between skeleton formats. In *IEEE/CVF Winter Conference on Applications of Computer Vision, WACV 2023, Waikoloa, HI, USA, January 2-7, 2023*, pages 2955–2965. IEEE, 2023. [2](#), [3](#)
- [19] István Sárádi, Timm Linder, Kai Oliver Arras, and Bastian Leibe. Metrabs: metric-scale truncation-robust heatmaps for absolute 3d human pose estimation. *IEEE Transactions on Biometrics, Behavior, and Identity Science*, 3(1):16–30, 2020. [2](#), [3](#)
- [20] Wenkang Shan, Zhenhua Liu, Xinfeng Zhang, Shanshe Wang, Siwei Ma, and Wen Gao. P-stmo: Pre-trained spatial temporal many-to-one model for 3d human pose estimation. In *European Conference on Computer Vision*, pages 461–478. Springer, 2022. [1](#), [2](#), [7](#), [8](#)
- [21] Xiao Sun, Bin Xiao, Fangyin Wei, Shuang Liang, and Yichen Wei. Integral human pose regression. In *Proceedings of the European conference on computer vision (ECCV)*, pages 529–545, 2018. [2](#)
- [22] Zhenhua Tang, Zhaofan Qiu, Yanbin Hao, Richang Hong, and Ting Yao. 3d human pose estimation with spatio-temporal criss-cross attention. In *Proceedings of the IEEE/CVF Conference on Computer Vision and Pattern Recognition*, pages 4790–4799, 2023. [2](#), [7](#), [8](#)
- [23] Shuhei Tsuchida, Satoru Fukayama, Masahiro Hamasaki, and Masataka Goto. Aist dance video database: Multi-genre, multi-dancer, and multi-camera database for dance information processing. In *Proceedings of the 20th International Society for Music Information Retrieval Conference, ISMIR 2019, Delft, Netherlands, Nov. 2019*. [1](#), [3](#), [4](#), [7](#)
- [24] Zhe Wang, Daeyun Shin, and Charless C Fowlkes. Predicting camera viewpoint improves cross-dataset generalization for 3d human pose estimation. In *Computer Vision—ECCV 2020 Workshops: Glasgow, UK, August 23–28, 2020, Proceedings, Part II 16*, pages 523–540. Springer, 2020. [3](#)
- [25] Ailing Zeng, Xiao Sun, Lei Yang, Nanxuan Zhao, Minhao Liu, and Qiang Xu. Learning skeletal graph neural networks for hard 3d pose estimation. In *Proceedings of the IEEE/CVF international conference on computer vision*, pages 11436–11445, 2021. [1](#), [2](#)
- [26] Weichen Zhang, Zhiguang Liu, Liuyang Zhou, Howard Lung, and Antoni B Chan. Martial arts, dancing and sports dataset: A challenging stereo and multi-view dataset for 3d human pose estimation. *Image and Vision Computing*, 61:22–39, 2017. [1](#), [3](#), [4](#), [7](#)
- [27] Ce Zheng, Sijie Zhu, Matias Mendieta, Taojiannan Yang, Chen Chen, and Zhengming Ding. 3d human pose estimation with spatial and temporal transformers. In *Proceedings of the IEEE/CVF International Conference on Computer Vision*, pages 11656–11665, 2021. [1](#), [2](#)

- [28] Kun Zhou, Xiaoguang Han, Nianjuan Jiang, Kui Jia, and Jiangbo Lu. Hemlets pose: Learning part-centric heatmap triplets for accurate 3d human pose estimation. In *2019 IEEE/CVF International Conference on Computer Vision, ICCV 2019, Seoul, Korea (South), October 27 - November 2, 2019*, pages 2344–2353. IEEE, 2019. [2](#), [3](#)